ORGANOMETALLICS

Article

pubs.acs.org/Organometallics

Reactivity of (Pyridine-Diimine)Fe Alkyl Complexes with Carbon Dioxide

Ka-Cheong Lau and Richard F. Jordan*

Department of Chemistry, The University of Chicago, 5735 South Ellis Avenue, Chicago, Illinois 60637, United States

Supporting Information

ABSTRACT: The reaction of CO_2 with (PDI)FeMe (**1**), (PDI)Fe(Me)-PMe_3 (**1-PMe$_3$**) and [(PDI)FeMe][BPh_4] (**2**, PDI = 2,6-(2,6-^{i}Pr$_2$−C_6H_3−N=CMe)$_2$−C_5H_3N) generates (PDI)FeOAc (**3**), (PDI)Fe(OAc)PMe_3 (**3-PMe$_3$**), and [(PDI)FeOAc][BPh_4] (**4**), respectively. Kinetic data and solvent effects provide evidence that these reactions occur by precoordination of CO_2 to the Fe center regardless of the charge state and thus favor an insertion mechanism for carboxylation. Carboxylation of **1-PMe$_3$** requires initial dissociation of PMe_3 to generate **1**, which reacts with CO_2; **1-PMe$_3$** itself does not react directly with CO_2. CO_2 reacts 5 times faster with neutral **1** than with cationic **2** (at 0 °C), which is ascribed to the higher nucleophilicity of the Fe−Me group in **1**.

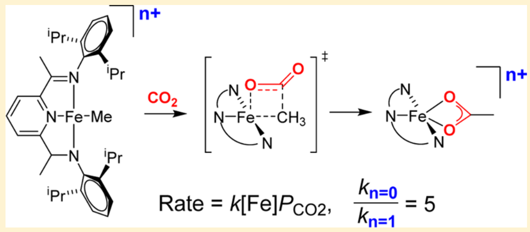

■ INTRODUCTION

The reaction of metal alkyls with CO_2 to afford metal carboxylate products plays a key role in strategies to convert CO_2 to value-added chemicals.[1−3] Mechanistic studies of these reactions may provide insights that are useful for the development of new CO_2 conversion processes. Experimental and computational studies show that the carboxylation of metal alkyls can occur by two general mechanisms (Scheme 1): (i) migratory insertion, involving initial CO_2 coordination to the metal center, followed by migration of the alkyl group via a four-center transition state, and (ii) S_E2 or S_Ei electrophilic substitution processes in which CO_2 directly attacks the metal alkyl carbon without prior coordination.

Scheme 1

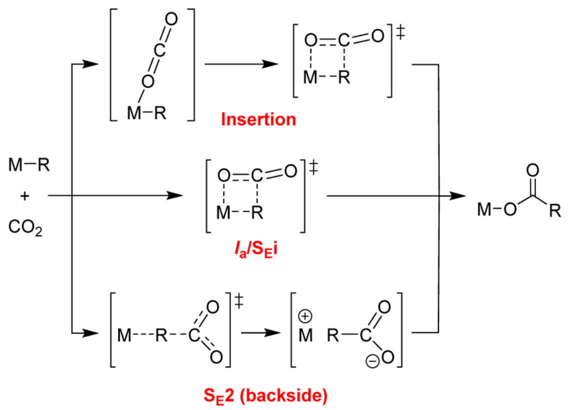

Reactivity and computational studies show that cationic $Cp_2ZrMe\{MeB(C_6F_5)_3\}$ and [$Cp_2ZrMe(ClC_6D_5)$][$B(C_6F_5)_4$], and neutral Cp_2ZrMe_2, react with CO_2 by insertion mechanisms to afford the corresponding acetate products.[4] The cationic complexes exhibit much higher reactivity due to the presence of the labile $MeB(C_6F_5)_3^-$ or C_6D_5Cl ligands, which facilitates CO_2 binding, and the cationic charge, which engenders stronger Zr···*O*CO interactions compared to neutral Cp_2ZrMe_2. Carboxylation reactions of other d^0 metal alkyls species likely proceed by similar mechanisms.[5] Kinetic studies show that dissociation of PMe_3 is required for carboxylation of the oxa-ruthenacycle Ru(PMe_3)$_4$(κ^2-*O*,*C*-OC_6H_3Me), consistent with a migratory insertion pathway.[6] In contrast, reactivity trends and computational studies show that carboxylation of group 10 metal (^{tBu}PCP)MMe pincer complexes ([^{tBu}PCP]$^-$ = [2,6-(^{t}Bu$_2$PCH$_2$)$_2$−C_6H_3]$^-$; M = Pd, Ni) occurs by direct S_E2 backside attack of CO_2 on the M−*Me* group to generate a M$^+$ ^-O_2CMe ion pair that collapses to the product. In these cases, the nucleophilicity of the M−*Me* group controls the reactivity.[7] Similarly, CO_2 reacts with (PO-^{i}Pr)PdMe$_2^-$ (PO-^{i}Pr$^-$ = 2-P^{i}Pr$_2$-4-Me−$C_6H_3SO_3^-$) to yield (PO-^{i}Pr)PdMe(OAc)$^-$ by direct S_E2 attack of CO_2 at the Pd−*Me* group that is *trans* to the phosphine, which is more electron-rich than the methyl group that is *cis* to the phosphine.[4b]

The most thoroughly studied carboxylation reactions are those of group 6 *cis*-M(CO)$_4$(L)R$^-$ complexes (M = Cr, W; L = CO, P(OMe)$_3$, PMe_3; R = Me, Et, Ph), which yield *cis*-M(CO)$_4$L(O_2CR)$^-$ products.[8] Darensbourg and co-workers showed that these reactions are accelerated by electron-donating ligands (L = PMe_3 > P(OMe)$_3$ > CO), proceed with retention of configuration at the alkyl carbon, and are not retarded by excess CO and thus do not proceed via a coordinatively unsaturated intermediate. On the basis of these and other observations, Darensbourg proposed a concerted I_a (associative interchange) mechanism, which may also be

Received: June 10, 2016

categorized as an S_Ei (internal electrophilic substitution) mechanism, for these reactions. In this mechanism, the CO_2 attacks the metal alkyl carbon with the involvement of a M···OCO interaction, but a M(OCO) adduct is not formed prior to the transition state (Scheme 1). Similar mechanisms have been implicated for Ru,[9] Rh,[10] and Cu[11] alkyls.

Here, we describe the reactions of the (pyridine-diimine)Fe alkyl complexes (PDI)FeMe (**1**), (PDI)Fe(Me)PMe_3 (**1-PMe$_3$**), and [(PDI)FeMe][BPh_4] (**2**, PDI = 2,6-(2,6-$^i Pr_2$–C_6H_3–N=CMe)$_2$–C_5H_3N) with CO_2. (Pyridine-diimine)Fe complexes have been used in olefin polymerization,[12] and many other catalytic reactions.[13] (PDI)FeMe and (PDI)$FeMe^+$ are unusual examples of metal alkyl species that have the same composition and nearly the same structure but differ in overall charge due to the presence of the redox-active PDI ligand. Thus, this system provides an interesting opportunity to probe how charge influences the carboxylation process. The reactions of several other Fe alkyl complexes with CO_2 have been reported.[14]

■ RESULTS AND DISCUSSION

Synthesis of (PDI)Fe Methyl Complexes. Complexes **1** and **2** were synthesized by the procedures reported by Chirik (Scheme 2).[15,16] Mössbauer spectroscopy, X-ray diffraction, and magnetic measurements show that **1** and **2** contain high-spin Fe^{2+} centers (S_{Fe} = 2), with a monoreduced PDI^- radical anion in **1** (S_{PDI} = $^1/_2$) and a neutral PDI ligand in **2** (S_{PDI} = 0).[17]

Scheme 2

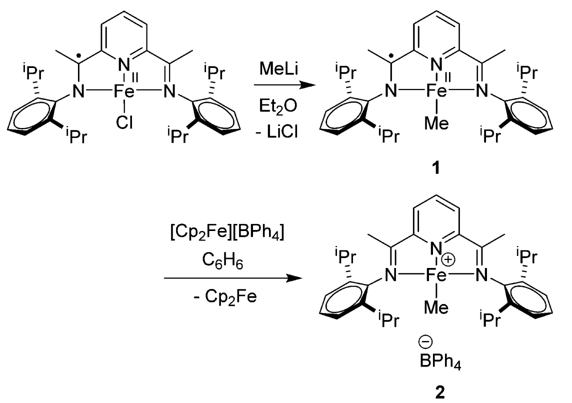

Synthesis of (PDI)Fe(Me)PMe$_3$. The reaction of **1** with PMe_3 yields the PMe_3 adduct **1-PMe$_3$** (Scheme 3). **1-PMe$_3$** is an unusual example of a (PDI)FeXL species with anionic X (Me) and neutral L (PMe_3) ligands, two other examples being (PDI)FeBr(THF) and {2,6-(2,6-Et_2–C_6H_3–N=CMe)$_2$–C_5H_3N}FeCl(OEt_2).[15,18] The solid state structure of **1-PMe$_3$** was characterized by X-ray diffraction, although the precision of the analysis is limited by a whole body disorder (see the Experimental Section and Supporting Information). In the solid state, **1-PMe$_3$** adopts a square-pyramidal structure, with the PMe_3 ligand bound in the axial position (Figure 1). This structure is analogous to those of (PDI)FeBr(THF) and {2,6-(2,6-Et_2–C_6H_3–N=CMe)$_2$–C_5H_3N}FeCl(OEt_2), which also adopt square-pyramidal geometries, with the THF and Et_2O ligands in axial positions. The Fe atom of **1-PMe$_3$** is displaced by 0.05(1) Å out of the plane formed by the PDI ligand and the Fe–*Me* group toward the PMe_3 ligand. The N_{imine}–C_{imine} (1.36(1) Å) and C_{imine}–C_{ipso} (1.42(1) Å) distances in **1-PMe$_3$** are similar to those in **1** (N_{imine}–C_{imine} = 1.335(7) Å, C_{imine}–C_{ipso} = 1.435(8) Å)[15] and are consistent with the presence of a reduced PDI ligand, although the low precision of the data precludes definitive assignment of the PDI oxidation state. The Fe–Me distance in **1-PMe$_3$** (2.00(4) Å) is also similar to that in **1** (2.001(6) Å). SQUID measurements establish that **1-PMe$_3$** has an effective magnetic moment of μ_{eff} = 1.8 μ_B, indicative of one unpaired electron. The X-band EPR spectrum of **1-PMe$_3$** in a toluene glass at 15 K gives a rhombic signal, with g_{min} = 2.050, g_{mid} = 2.075, g_{max} = 2.224, showing that there is significant spin density at the Fe center. On the basis of these results, we assign **1-PMe$_3$** an electronic configuration comprising a PDI^- radical anion (S_{PDI} = $^1/_2$) that is antiferromagnetically coupled with an intermediate spin state Fe^{2+} center (S_{Fe} = 1).

Scheme 3

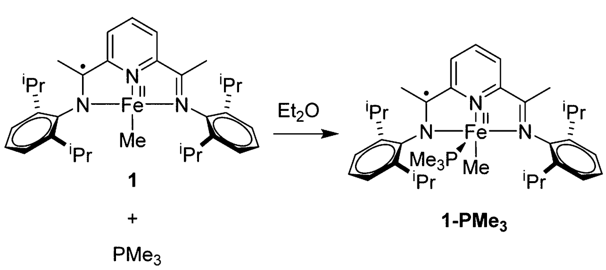

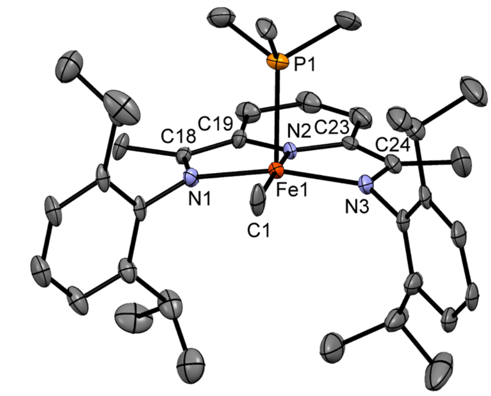

Figure 1. Molecular structure of (PDI)Fe(Me)PMe_3 (**1-PMe$_3$**). Selected bond lengths (Å) and angles (deg): Fe1–C1 2.00(4), Fe1–P1 2.359(8), Fe1–N1 1.962(9), Fe1–N2 1.874(10), Fe1–N3 1.955(10), N1–C18 1.356(11), C18–C19 1.414(11), N3–C24 1.354(13), C24–C23 1.423(11), C1–Fe1–P1 101.1(14), N1–Fe1–C1 96.8(13), N2–Fe1–C1 174.2(15), N3–Fe1–C1 101.7(12), N1–Fe1–P1 97.8(4), N2–Fe1–P1 84.3(4), N3–Fe1–P1 98.6(4), N2–Fe1–N1 80.1(4), N2–Fe1–N3 79.5(5).

The ^1H NMR spectrum of **1-PMe$_3$** in C_6D_6 exhibits concentration-dependent behavior. Upon dilution of the solution, the ^1H resonances for **1-PMe$_3$** shift toward the chemical shifts of base-free **1** and free PMe_3 (Figure 2). Addition of excess PMe_3 to **1-PMe$_3$** shifts the ^1H resonances for **1-PMe$_3$** away from the chemical shifts of **1** but also broadens them significantly. In addition, the ^1H NMR spectra of mixtures of **1** and **1-PMe$_3$** contain a single set of resonances at the mole-fraction-weighted average of the chemical shifts of **1** and **1-PMe$_3$** (Figure 3). These results show that **1-PMe$_3$** undergoes partial dissociation of PMe_3 to form **1**, and that **1**

DOI: 10.1021/acs.organomet.6b00470
Organometallics XXXX, XXX, XXX−XXX

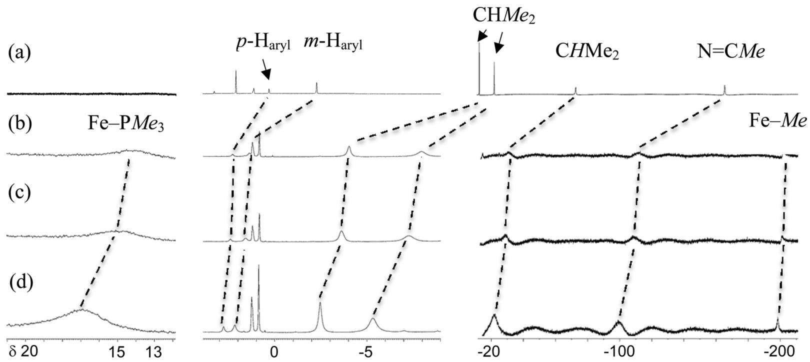

Figure 2. ^{1}H NMR spectra of (a) **1** (0.029 M) in toluene-d_8, (b) **1-PMe$_3$** (0.010 M) in C_6D_6, (c) **1-PMe$_3$** (0.012 M) in C_6D_6, and (d) **1-PMe$_3$** (0.026 M) in C_6D_6, at 23 °C. Three key regions of the spectra are shown: δ 21−12, δ 5 to −9, and δ −20 to −210; note that the horizontal expansion of each region is different. The variation of chemical shifts of the resonances of **1-PMe$_3$** with concentration and the correlations of these resonances with those for **1** are indicated by dashed lines. Other resonances: δ 3.3 (Et_2O), 1.3 (pentane), 1.2 (Et_2O), 0.9 (pentane). The chemical shift of free PMe_3 (which is not present) is δ 0.8.

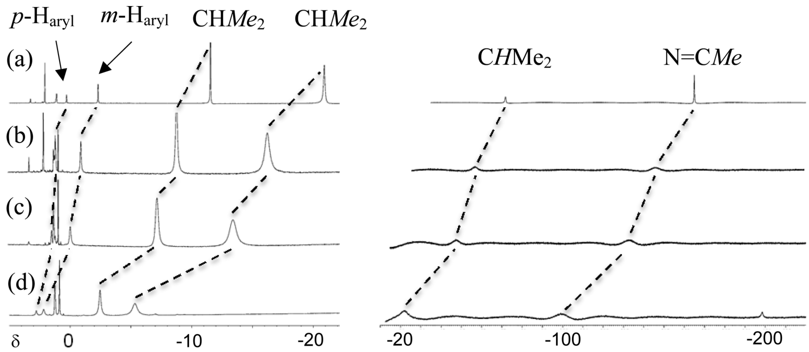

Figure 3. ^{1}H NMR spectra of (a) **1** (0.029 M) in toluene-d_8, (b) a 1/3 mixture of **1-PMe$_3$** and **1** (0.016 M total) in toluene-d_8, (c) a 1/1 mixture of **1-PMe$_3$** and **1** (0.040 M total) in C_6D_6, and (d) **1-PMe$_3$** (0.026 M) in C_6D_6, at 23 °C. Two key regions of the spectra are shown: δ 5 to −22 and δ −10 to −220; note that the horizontal expansion of each region is different. The correlations of the resonances of **1-PMe$_3$** and **1** are indicated by dashed lines. Other resonances: δ 3.3 (Et_2O), 2.1 (toluene-d_7), 1.3 (pentane), 1.2 (Et_2O), 0.9 (pentane), −198.4 (Fe−*Me* of **1-PMe$_3$**).

and **1-PMe$_3$** undergo rapid exchange on the NMR time scale (Scheme 4). The equilibrium constant for PMe_3 dissociation of **1-PMe$_3$** was determined to be $K_{eq} = 1.8(9) \times 10^{-3}$ M at 23 °C using the method of Rose and Drago.[19]

Scheme 4

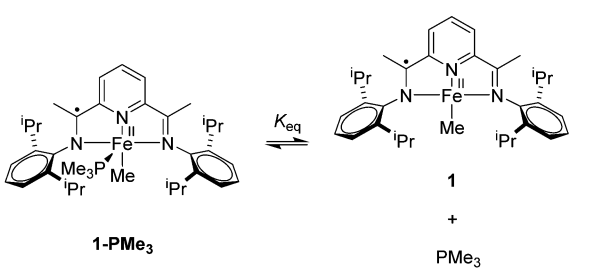

The ^{1}H NMR spectrum of **1** has been assigned by Chirik and co-workers by analysis of peak intensities and the ^{1}H and ^{2}H NMR spectra of ^{2}H-labeled samples.[15,20] The ^{1}H resonances for **1-PMe$_3$** were assigned by correlating the resonances of **1**, **1-PMe$_3$**, and rapidly exchanging mixtures of these species as shown in Figure 3. For example, the two CH*Me*$_2$ resonances of **1** at δ −21 and −11 (Figure 3a) move steadily to δ −5 and −3 as the **1-PMe$_3$**/**1** ratio is increased, implying that the δ −5 and −3 resonances of **1-PMe$_3$** are due to the CH*Me*$_2$ groups. The resonance at δ 17 for **1-PMe$_3$** (Figure 2) was assigned to the PMe_3 ligand because this resonance is not correlated with any resonance for **1** and moves toward the chemical shift of free PMe_3 (δ 0.8) as the solution of **1-PMe$_3$** is diluted. The resonance at δ −198.4 for **1-PMe$_3$** was assigned to the Fe−*Me* group based on the observations that this resonance disappears upon mixing **1-PMe$_3$** with **1** and the Fe−*Me* resonance of **1** is not observable.

Carboxylation of 1. Complex **1** reacts with CO_2 in C_6D_6 at room temperature to afford the known acetate complex (PDI)FeOAc (**3**, Scheme 5), which was previously characterized by Chirik and co-workers.[20] No intermediates in this reaction were detected by NMR. The kinetics of the reaction of **1** with CO_2 in toluene-d_8 were measured by ^{1}H NMR spectroscopy by monitoring the disappearance of the CH*Me*$_2$ resonance (δ −11) of **1** (Figure 4). The reaction is first-order in **1** and CO_2 (Figure 5)

Scheme 5

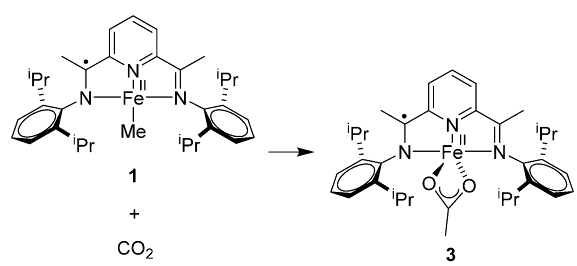

DOI: 10.1021/acs.organomet.6b00470
Organometallics XXXX, XXX, XXX−XXX

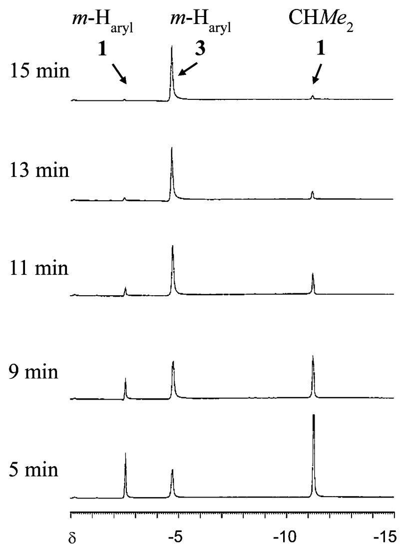

Figure 4. ¹H NMR monitoring of the reaction of **1** with CO_2 (1 atm) in toluene-d_8 at 0 °C. Selected spectra are shown. These spectra show the disappearance of **1** and concomitant formation of **3**.

$$\text{rate} = k_1'[\mathbf{1}] = k_1[\mathbf{1}]P_{CO_2}$$

where k_1' is the observed first-order rate constant, k_1 is the second-order rate constant, and P_{CO_2} is the pressure of CO_2.

The observed first-order rate constant at 0 °C and P_{CO_2} = 1 atm was determined to be $k_1' = 3.63(9) \times 10^{-3}$ s^{-1}. k_1 values for the conversion of **1** to **3** (P_{CO_2} = 1 atm) were determined over the temperature range of 0 to −35 °C. An Eyring plot is shown in Figure 6, and activation parameters are listed in Table 1. Extrapolation from the Eyring plot gave k_1 (23 °C) = 2(4) × 10^{-2} atm^{-1} s^{-1}.

Carboxylation of 1-PMe$_3$. As noted earlier, carboxylation reactions of metal alkyl complexes that proceed by insertion mechanisms require a vacant site for CO_2 binding and, therefore, are expected to be inhibited or quenched by addition of competing ligands. In contrast, carboxylation reactions that proceed by I_a or S_E2 mechanisms do not require a vacant site but do require a nucleophilic alkyl ligand, and these reactions are expected to be unaffected or possibly accelerated by electron-donating ligands. Accordingly, comparison of the carboxylation reactions of **1** and **1-PMe$_3$** may provide insight into the mechanism of carboxylation of the former complex.

The reaction of **1-PMe$_3$** with CO_2 in C_6D_6 proceeds at room temperature to form the acetate complex (PDI)Fe(OAc)PMe$_3$ (**3-PMe$_3$**), which exists in equilibrium with its PMe$_3$-dissociated form **3** and PMe$_3$ (Scheme 6). No intermediates in this reaction were detected by NMR. **3-PMe$_3$** was independently generated by the reaction of **3** with PMe$_3$.

Vacuum transfer of the volatiles from a solution of **3-PMe$_3$** in C_6D_6 afforded 0.9 equiv of PMe$_3$ in the volatile fraction and essentially pure **3** in the nonvolatile fraction, as determined by ¹H and ³¹P NMR, indicating that the PMe$_3$ of **3-PMe$_3$** is quite labile. The ¹H NMR spectrum of **3-PMe$_3$** in C_6D_6 at room temperature is only slightly shifted from that of base-free **3** (Δδ ca. 1−2 ppm), and no PMe$_3$ resonance is observed for **3-PMe$_3$** by ¹H or ³¹P NMR. These observations indicate that the PMe$_3$ ligand of **3-PMe$_3$** undergoes extensive dissociation and fast exchange. The differences in the observed ¹H NMR chemical shifts of **3** and **3-PMe$_3$** are too small to allow accurate

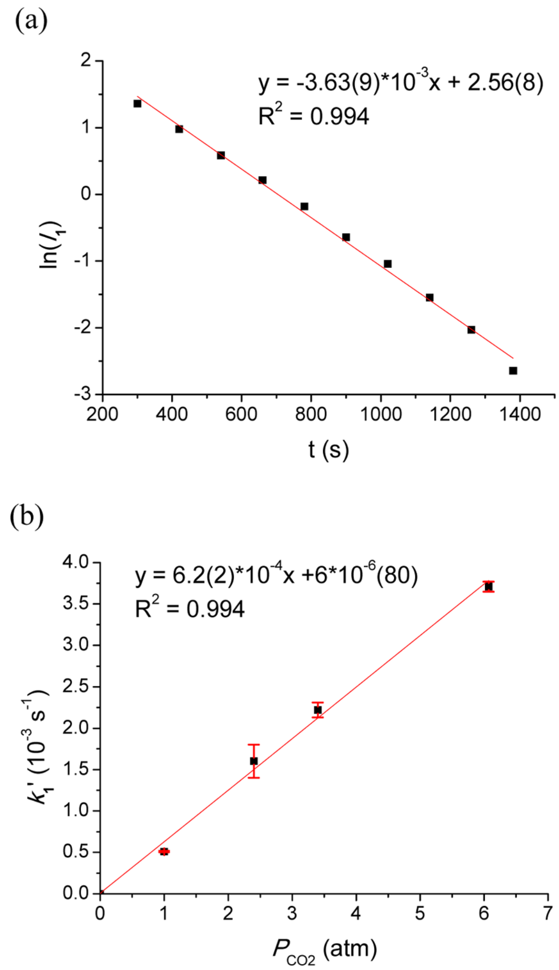

Figure 5. Representative kinetic plots for the reaction of **1** with CO_2 in toluene-d_8. (a) Plot of ln(I_1) versus time (0 °C, P_{CO_2} = 1 atm); I_1 = integral value for the CHMe_2 resonance of **1** at δ −11 relative to the integral value of the Et_2O resonance (δ 1.2, internal standard). (b) Plot of k_1' vs P_{CO_2} (−25 °C).

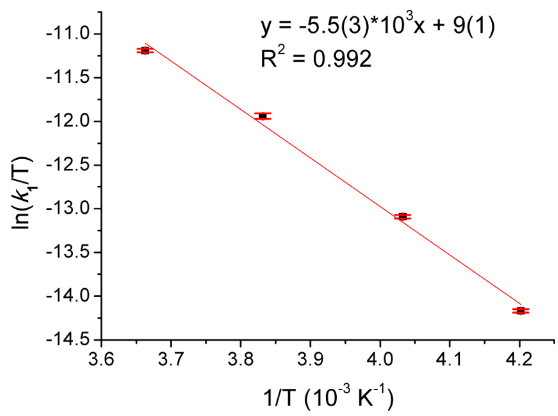

Figure 6. Eyring plot for the reaction of **1** with CO_2 (1 atm) in toluene-d_8.

Table 1. Activation Parameters for the Reaction of CO_2 (1 atm) with 1 and 2

	$\Delta H^\ddagger$ (kcal/mol)	$\Delta S^\ddagger$ (e.u.)	$\Delta G^\ddagger$ at 0 °C (kcal/mol)
1	10.9(6)	−29(2)	19(1)
2	14.9(9)	−17(3)	20(2)

DOI: 10.1021/acs.organomet.6b00470
Organometallics XXXX, XXX, XXX−XXX

Scheme 6

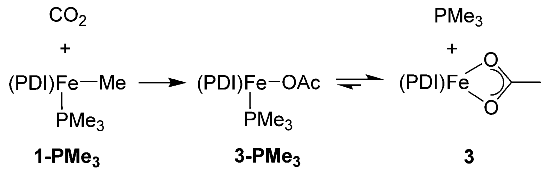

determination of K_{eq}. Addition of excess PMe_3 to shift the equilibrium to **3-PMe$_3$** shifts the ^{1}H NMR resonances of **3-PMe$_3$** away from those of **3** but also broadens them significantly. **3-PMe$_3$** could not be isolated.

Kinetics of Carboxylation of 1-PMe$_3$. The observation that **1-PMe$_3$** undergoes partial dissociation of PMe_3 in solution raises the question of whether the observed reaction of **1-PMe$_3$** and CO_2 to form **3-PMe$_3$** proceeds by direct carboxylation of **1-PMe$_3$** or requires prior PMe_3 dissociation. The kinetics of the reaction of **1-PMe$_3$** with CO_2 (1 atm) in the presence of excess PMe_3 were studied to address this issue. Due to the broadening of the resonances of **1-PMe$_3$** in the presence of PMe_3 noted above, the kinetics were measured by analyzing the appearance of **3-PMe$_3$**, monitoring the CHMe_2 resonance at δ −18 (Figure 7).

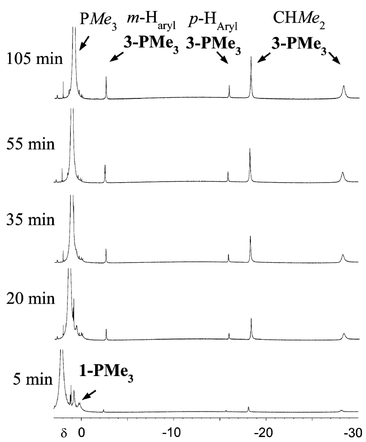

Figure 7. ^{1}H NMR monitoring of the reaction of **1-PMe$_3$** with CO_2 (1 atm) in the presence of excess PMe_3 (0.04 M) in C_6D_6 at 23 °C. k_{obs} (23 °C) = 6.9(3) × 10^{-4} s^{-1}. One resonance for **1-PMe$_3$** is visible at δ 0, and the others are broadened into the baseline due to the presence of excess PMe_3. Other resonance: δ 1.1 (t, Et_2O).

The carboxylation of **1-PMe$_3$** is first-order in the total concentration of Fe−Me species, i.e.

$$\text{Rate} = k_{obs}[\text{Fe–Me}] = k_{obs}([\mathbf{1\text{-}PMe_3}] + [\mathbf{1}])$$

where k_{obs} = observed first-order rate constant and [Fe−Me] = [**1-PMe$_3$**] + [**1**].

The first-order rate equation for the appearance of **3-PMe$_3$** (exponential form) is given by

$$I_{Fe} = I_{Fe,\infty}[1 - \exp(-k_{obs}t)]$$

where I_{Fe} and $I_{Fe,\infty}$ are the integral values of the δ −18 resonance of **3-PMe$_3$** (relative to that of an internal standard) at time = t and the end of the reaction, respectively. A representative kinetic plot is shown in Figure 8. The conversion of **1-PMe$_3$** to **3-PMe$_3$** is strongly inhibited by PMe_3 (Table 2).

A pre-equilibrium reaction scheme consistent with these results and the known dissociation of PMe_3 from **1-PMe$_3$** is shown in Scheme 7. In Scheme 7, reversible dissociation of PMe_3 from **1-PMe$_3$** generates an equilibrium mixture of **1**, **1-PMe$_3$**, and PMe_3. **1** reacts with CO_2 to form **3**, which, in the presence of PMe_3, gives **3-PMe$_3$**. **1-PMe$_3$** does not react directly with CO_2.

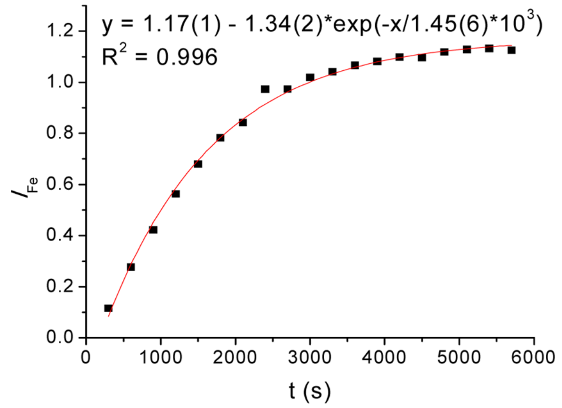

Figure 8. Representative first-order kinetic plot for the formation of **3-PMe$_3$** from the reaction of **1-PMe$_3$** with CO_2 (1 atm) in C_6D_6 at 23 °C in the presence of 0.04 M free PMe_3. k_{obs} = 6.9(3) × 10^{-4} s^{-1}.

Table 2. Observed First-Order Rate Constants (k_{obs}) for the Reaction of 1-PMe$_3$ with CO$_2$ (1 atm) and Various [PMe$_3$] Values at 23 °C

[PMe_3] (M)	k_{obs} (10^{-4} s^{-1})
0.04	6.9(3)
0.05	5.7(2)
0.09	3.1(1)
0.11	2.6(2)
0.13	2.35(6)
0.17	1.69(8)

Scheme 7

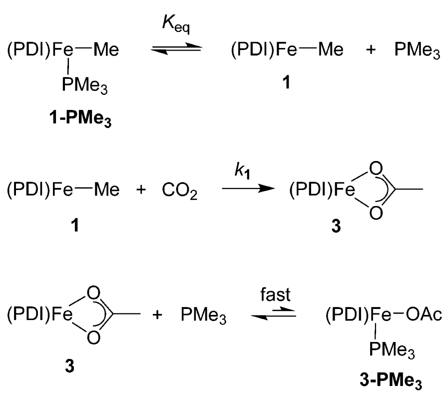

The rate equation for this mechanism is

$$\text{rate} = k_{obs}[\text{Fe–Me}]$$

where

$$k_{obs} = \frac{k_1 P_{CO_2} K_{eq}}{K_{eq} + [PMe_3]}$$

and

$$[\text{Fe–Me}] = [\mathbf{1\text{-}PMe_3}] + [\mathbf{1}]$$

DOI: 10.1021/acs.organomet.6b00470
Organometallics XXXX, XXX, XXX−XXX

Rearranging, and at $P_{CO_2} = 1$ atm

$$\frac{1}{k_{obs}} = \frac{1}{k_1K_{eq}}[PMe_3] + \frac{1}{k_1} \quad (1)$$

A plot of $1/k_{obs}$ versus $[PMe_3]$ over the range of $[PMe_3]$ = 0.04−0.17 M is shown in Figure 9. Consistent with Scheme 7 and eq 1, the plot is linear and gives k_1 (23 °C) = 2(3) × 10^{-2} atm^{-1} s^{-1} and K_{eq} (23 °C) = 2(3) × 10^{-3} M. Importantly, these results are in excellent agreement with the values determined independently by the kinetic studies of **1** and the ^1H NMR analysis of **1-PMe$_3$** (k_1 = 2(4) × 10^{-2} atm^{-1} s^{-1} and K_{eq} = 1.8(9) × 10^{-3} M), which confirms the mechanism in Scheme 7, and, in particular, that **1-PMe$_3$** does not react directly with CO_2 under these conditions.

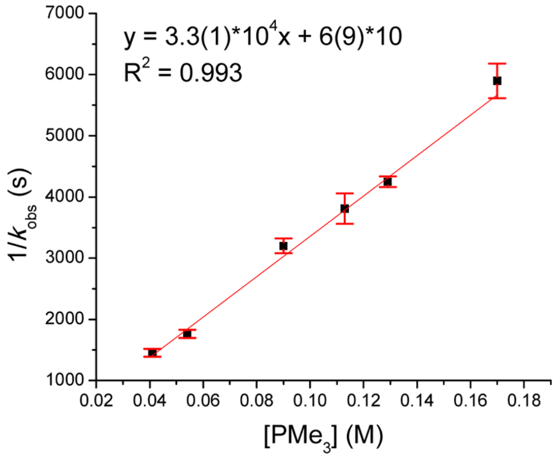

Figure 9. Plot of $1/k_{obs}$ versus $[PMe_3]$ for the reaction of **1-PMe$_3$** with CO_2 (1 atm) to produce **3-PMe$_3$** in C_6D_6 at 23 °C.

Carboxylation of 2 in a Noncoordinating Solvent. The reaction of cationic complex **2** with CO_2 in C_6D_5F at room temperature affords [(PDI)FeOAc][BPh_4] (**4**, Scheme 8). No intermediates in this reaction were detected by NMR. Complex **4** was independently synthesized by the oxidation of **3** with [Cp_2Fe][BPh_4] and characterized by X-ray diffraction (Figure 10). The (PDI)Fe(OAc)$^+$ cation of **4** is structurally similar to the neutral analogue **3**.[20] The coordination geometry at the Fe center of **4** is trigonal-bipyramidal, as observed for **3**. The acetate unit is bound in a symmetrical κ^2 fashion, and the plane of the acetate unit is orthogonal to the (PDI)Fe chelate plane. The Fe−O bond distances in **4** are ca. 0.04 Å shorter than those in **3** (2.1271(14), 2.0837(16) Å), which is expected for stronger Fe−O bonding in cationic **4** versus neutral **3**. The bond lengths within the PDI ligand of **4** are consistent with a neutral (nonreduced) PDI ligand. A SQUID analysis gave μ_{eff} = 5.3 μ_B, indicative of 4 unpaired electrons in **4**. These results are consistent with the presence of a high-spin Fe^{2+} (S_{Fe} = 2) with neutral PDI ligand (S_{PDI} = 0) in **4**. The IR ν_{CO} values for **4** (ν_{asym} = 1548 cm^{-1}, ν_{sym} = 1472 cm^{-1}, $\Delta\nu_{CO} = \nu_{asym} - \nu_{sym}$ = 76 cm^{-1}) are also consistent with a κ^2 binding mode for the acetate ligand.[21]

Scheme 8

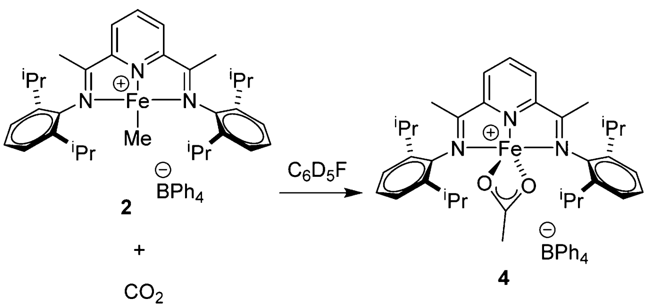

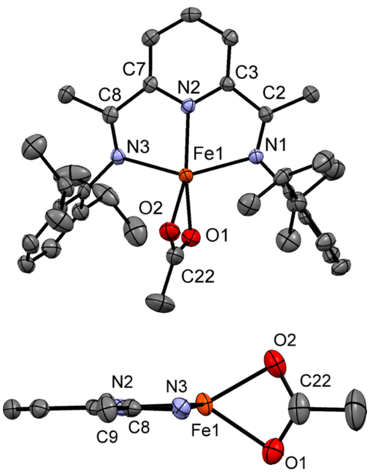

Figure 10. Two views of the molecular structure of [(PDI)FeOAc]-[BPh_4] (**4**). The BPh_4^- anion and hydrogen atoms are omitted in both views and the 2,6-$^iPr_2$−C_6H_3 groups are omitted in the side view. Selected bond lengths (Å) and angles (deg): Fe1−O1 2.0869(19), Fe1−O2 2.0462(19), Fe1−N1 2.153(2), Fe1−N2 2.082(2), Fe1−N3 2.169(2), N1−C2 1.282(3), C2−C3 1.492(4), N3−C8 1.276(3), C8−C7 1.493(4), O2−Fe1−O1 63.94(9), N1−Fe1−O1 104.35(8), N1−Fe1−O2 109.93(8), N2−Fe1−O1 143.44(9), N2−Fe1−O2 151.91(8), N3−Fe1−O1 98.36(8), N3−Fe1−O2 99.47(8), N2−Fe1−N1 74.36(8), N2−Fe1−N3 74.41(8), N3−Fe1−N1 148.53(8).

The kinetics of the reaction of **2** with CO_2 were measured by ^1H NMR spectroscopy, monitoring the disappearance of the δ −25 resonance of **2** (Figure 11). The reaction is first-order in **2** and CO_2 (see Figures S-7 and S-8 in the Supporting Information)

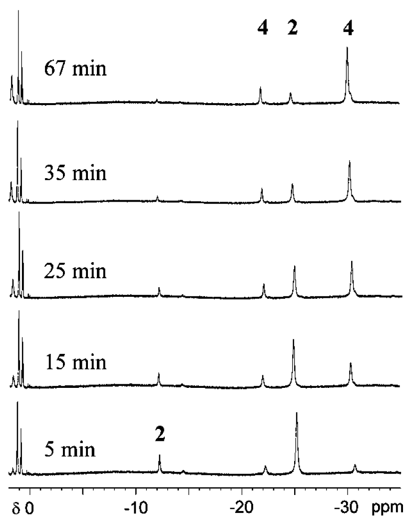

Figure 11. ^1H NMR monitoring of the reaction of **2** with CO_2 (1 atm) in C_6D_5F at 0 °C to produce **4**. Other resonances: δ 1.2 (pentane), 0.9 (pentane).

DOI: 10.1021/acs.organomet.6b00470
Organometallics XXXX, XXX, XXX−XXX

$$\text{rate} = k_2'[\mathbf{2}] = k_2[\mathbf{2}]P_{CO_2}$$

where k_2' is the observed first-order rate constant and k_2 is the second-order rate constant.

The value for k_2' at 0 °C and P_{CO_2} = 1 atm is $k_2' = 7.10(9) \times 10^{-4}$ s^{-1}. Therefore, under these conditions, the carboxylation of **2** is 5-fold *slower* than that of **1** (k_1' (0 °C) = $3.63(9) \times 10^{-3}$ s^{-1}).

Values for k_2 for the conversion of **2** to **4** were determined over the temperature range of 23 to −10 °C, and activation parameters determined from an Eyring plot are given in Table 1 (see Figure S-9 in the Supporting Information).

Carboxylation of 2 in a Coordinating Solvent. To probe whether CO_2 precoordination to the Fe center is important for the carboxylation of **2**, the reaction of **2** with CO_2 (1 atm) was carried out in the coordinating solvent THF-d_8 at room temperature. Several observations show that **2** binds THF to form, presumably, **2-THF**. First, the color of a solution of **2** in C_6D_5F changes from red to blue upon addition of THF, consistent with the color change associated with the conversion of the analogous alkyl complexes [(PDI)FeR][BPh_4] to [(PDI)FeR(THF)][BPh_4] (R = CH_2CMe_3, CH_2SiMe_3).[16,22] Second, the ^{1}H NMR spectrum of **2** in THF-d_8 is significantly shifted from that of **2** in C_6D_5F (see Figure S-2 in the Supporting Information). ^{1}H NMR monitoring experiments show that **2** *does not* react with CO_2 to produce **4** in THF-d_8 at room temperature but rather partially decomposes over time. The rate of decomposition is approximately the same as that in the absence of CO_2. These results show that the coordination of THF to **2** blocks the carboxylation reaction.

Comparative Reactivity of 1, 2, and Other Metal Alkyls with CO_2. The observation that PMe_3 and THF block the carboxylation of **1** and **2**, respectively, implies that these reactions proceed by initial coordination of CO_2 to the Fe center and thus favors an insertion mechanism in both cases. The similarity in the rates, activation parameters, and effects of added ligands of these reactions reflects the structural and electronic commonalities of **1** and **2**, both of which are square-planar, 4-coordinate, high-spin Fe^{II} species. The modest (5-fold) rate enhancement observed for **1** versus **2** can be ascribed to the presence of the reduced PDI ligand in the former species, which renders the Fe−*Me* group more nucleophilic than that in **2**.

Interestingly, while the carboxylation of **1** and **2** appears to require initial CO_2 coordination, consistent with an insertion process, the rate trend (**1** faster than **2**) is opposite to that observed for zirconocene species, which react with CO_2 by an insertion mechanism, and parallel to that for group 6 and 10 metal alkyls that react with CO_2 by I_a/S_E2 mechanisms. One explanation for this observation is that **1** and **2** have similar CO_2 binding properties and, as a result, the nucleophilic character of the Fe−*Me* group exerts a controlling influence on the carboxylation rate. These comparisons showcase the spectrum of mechanisms and reactivity trends that are possible for the carboxylation of metal alkyls.

■ CONCLUSION

(PDI)FeMe (**1**) and [(PDI)FeMe][BPh_4] (**2**) react with CO_2 to yield the corresponding acetate products (PDI)FeOAc (**3**) and [(PDI)FeOAc][BPh_4] (**4**). Donor ligands (PMe_3, THF) block these reactions, which implies that they proceed by initial coordination of CO_2 to the Fe center.

■ EXPERIMENTAL SECTION

General Procedures. All experiments were performed using drybox or Schlenk techniques under a nitrogen atmosphere. Nitrogen was purified by passage through activated molecular sieves and Q-5 oxygen scavenger. C_6D_5F and C_6H_5F were distilled from and stored over P_2O_5. C_6D_6, toluene-d_8, and THF-d_8 were distilled from Na/benzophenone. Pentane, hexanes, and toluene were purified by passage through activated alumina and BASF R3-11 oxygen scavenger. THF, CH_2Cl_2, and Et_2O were purified by passage through activated alumina. CO_2 (99.999%) was purchased from Airgas and used as received. [Cp_2Fe][BPh_4],[23] (PDI)FeCl, (PDI)FeMe (**1**),[15] and [(PDI)FeMe][BPh_4] (**2**)[16] were synthesized by literature procedures. NMR spectra were recorded on a Bruker DMX-500 spectrometer in Teflon-valved J. Young tubes at ambient temperature unless otherwise indicated. ^{1}H NMR chemical shifts are reported relative to $SiMe_4$ and were determined by reference to the residual ^{1}H solvent resonances. Mass spectrometry experiments were performed on Agilent 6224 TOF-MS (high resolution) or Agilent 6130 LCMS (low resolution) instruments. Magnetization data were recorded with a SQUID magnetometer (Quantum Design). Magnetic susceptibility values were corrected for the underlying diamagnetic increment by using tabulated Pascal constants and the effect of the blank sample holders. EPR spectra were collected on a Bruker Elexsys-II E500 spectrometer and simulated using Easyspin software.[24]

X-ray Crystallography. Crystallographic data are summarized in Table S-1 in the Supporting Information and the accompanying CIF files. Data were collected on a Bruker D8 Venture PHOTON 100 CMOS Diffractometer using Mo Kα radiation (0.71073 Å). Direct methods were used to locate many atoms from the E-map. Repeated difference Fourier maps allowed location of all expected non-hydrogen atoms. Following anisotropic refinement of all non-H atoms, ideal H atom positions were calculated. Final refinement was anisotropic for all non-H atoms, and isotropic-riding for H atoms. ORTEP diagrams are drawn with 40% probability ellipsoids. Specific comments for each structure are as follows. **1-PMe$_3$**: Crystals of **1-PMe$_3$** were obtained by crystallization from a saturated solution of **1-PMe$_3$** in pentane at −35 °C. Significant elongation of most of the thermal ellipsoids was observed and was modeled as a whole body disorder of two equivalent complexes sitting at almost the same location (ratio: 60/40). All atoms were refined with anisotropic thermal parameters utilizing constraints on thermal parameters (RIGU, SIMU, EADP). While geometric restraints were initially used to support the refinement, geometric parameters were not restrained during the final refinement cycles except for soft SADI restraints that were imposed on the ^{i}Pr groups. After modeling the disorder, the data/parameter ratio was about 9. **4**: Crystals of **4** were obtained by layering hexanes onto a solution of **4** in C_6H_5F at room temperature. No anomalous bond lengths or thermal parameters were noted.

(PDI)Fe(Me)PMe$_3$ (1-PMe$_3$). A solution of PMe_3 in Et_2O (0.098 M, 1.15 mL, 0.11 mmol) was added to a solution of **1** in Et_2O (0.054 M, 2.0 mL, 0.11 mmol), and the mixture was stirred at room temperature for 5 min. ^{1}H NMR analysis showed that an equilibrium mixture of **1-PMe$_3$** and **1** had formed. The volatiles were removed under vacuum to afford a brown solid. Recrystallization of the solid from a saturated pentane solution at −35 °C afforded dark green crystals that were identified by ^{1}H NMR and X-ray diffraction as **1-PMe$_3$** (45 mg, 0.072 mmol, 66%). ^{1}H NMR (C_6D_6, 0.027 M): δ 16.9 (Fe−PMe_3), 2.8 (p-H$_{aryl}$), 2.2 (m-H$_{aryl}$), −2.7 (CHMe_2), −5.3 (CHMe_2), −22.1 (CHMe$_2$), −100.2 (N═CMe), −198.4 (Fe−Me). μ_{eff} (SQUID, 27 °C): 1.8 μ_B. Multiple elemental analyses of crystalline samples of **1-PMe$_3$** gave irreproducible results for C but accurate results for H, N and P possibly due to incomplete combustion. Anal. Calcd for $C_{37}H_{55}FeN_3P$: C, 70.69; H, 8.82; N, 6.68; P, 4.93. Found: C, 69.81; H, 9.21; N, 6.49; P, 4.88.

Reversible Dissociation of PMe_3 from 1-PMe$_3$. An NMR tube was charged with **1-PMe$_3$** (8.0 mg, 0.013 mmol). C_6D_6 (0.5 mL) was added by vacuum transfer at −196 °C. The mixture was thawed at room temperature. This solution was serially diluted by addition of C_6D_6, and ^{1}H NMR spectra were recorded at each concentration.

DOI: 10.1021/acs.organomet.6b00470
Organometallics XXXX, XXX, XXX−XXX

Upon dilution, the ^{1}H NMR resonances for **1-PMe$_3$** shifted toward the chemical shifts of **1** and free PMe_3. These results are consistent with partial dissociation of PMe_3 to form **1**, and rapid exchange between **1-PMe$_3$** and **1** on the NMR time scale (Figure 2). The fast exchange between **1-PMe$_3$** and **1** was confirmed by ^{1}H NMR spectra of mixtures of **1-PMe$_3$** and **1** (Figure 3 and Figure S-1 in the Supporting Information). The ^{1}H NMR resonances for mixtures of **1-PMe$_3$** and **1** appear at the mole-fraction-weighted-averaged chemical shifts of the resonances of **1-PMe$_3$** and **1**.

Generation of [(PDI)Fe(Me)THF][BPh$_4$] (2-THF). An NMR tube was charged with **2** (8.7 mg, 0.010 mmol), and C_6D_5F (0.5 mL) was added by vacuum transfer at −196 °C. The mixture was thawed at room temperature to produce a red solution. THF (0.010 mmol) was added by syringe to afford a blue solution. The formation of **2-THF** is supported by several observations as discussed in the text (Figure S-2 in the Supporting Information). ^{1}H NMR (THF-d_8): δ 82.37, 78.79, 11.52, 8.70, 7.66, −4.17, −9.95, −34.84. ^{1}H NMR (C_6D_5F): δ 85.58, 81.26, 9.54, 8.18, 4.40, 2.35, 1.17, −5.67, −10.46, −42.71. **2-THF** is thermally unstable in THF-d_8 and C_6D_5F at room temperature and decomposed over 1 day to give a black precipitate.

(PDI)FeOAc (3). This compound was previously synthesized by the reaction of (PDI)Fe(N_2)$_2$ with EtOAc, or with MeOAc and H_2.[20] In the present work, **3** was prepared by carboxylation of **1**. A Schlenk flask was charged with **1** (210 mg, 0.379 mmol). The flask was evacuated and exposed to CO_2 (1 atm). Et_2O (10 mL) was added by syringe, and the mixture was stirred for 15 min at room temperature under a CO_2 atmosphere. The volatiles were removed under vacuum to afford **3** as a green solid (212 mg, 0.354 mmol, 93%). ^{1}H NMR data for **3** matched the literature data. IR ν_{CO} (KBr): 1515, 1459 cm^{-1}. IR assignments were made by inspection of the IR spectra of **3**, **3-^{13}C$_1$** (synthesized from **1** and $^{13}CO_2$), and (PDI)FeCl (Figure S-10 in the Supporting Information).

Generation of (PDI)Fe(OAc)PMe$_3$ (3-PMe$_3$). (a) An NMR tube was charged with **1-PMe$_3$** (5.2 mg, 0.0083 mmol). Toluene-d_8 (0.6 mL) was added by vacuum transfer at −196 °C. The mixture was thawed and exposed to CO_2 (1 atm, 12 equiv) at room temperature. The tube was agitated for 15 min at room temperature. ^{1}H NMR analysis showed that an equilibrium mixture of **3-PMe$_3$** and **3** had formed. These species exchange rapidly on the NMR time scale in toluene-d_8. The ^{1}H resonances for **3-PMe$_3$** were assigned using the approach described in the text for **1-PMe$_3$**. ^{1}H NMR (toluene-d_8, 0.017 M): δ 184.5 (OC(O)*Me*), 118.9 (*m*-py), −2.9 (*m*-Ar), −16.2 (*p*-Ar), −19.3 (CH*Me*$_2$), −29.7 (CH*Me*$_2$), −112.2 (C*H*Me$_2$), −282.4 (N═C*Me*); the Fe−P*Me*$_3$ resonance was not observed. (b) An NMR tube was charged with **3** (10.7 mg, 0.0179 mmol), and a solution of PMe_3 in C_6D_6 (0.036 M, 0.5 mL, 0.018 mmol) was added. The tube was agitated at room temperature for 5 min. ^{1}H NMR analysis showed that an equilibrium mixture of **3-PMe$_3$** and **3** had formed.

[(PDI)FeOAc][BPh$_4$] (4). Compound **3** (61 mg, 0.10 mmol) and [Cp_2Fe][BPh$_4$] (45 mg, 0.089 mmol) were taken up in benzene (5 mL), and the green slurry was stirred at room temperature for 45 min. Pentane (10 mL) was added, and the mixture was stirred for 15 min to afford an orange-red slurry. The yellow supernatant was removed by pipet, and the solid was washed with pentane until the washes were colorless. The solid was dried under vacuum to afford a pale red powder (81 mg, 0.088 mmol, 99%). The use of a substoichiometric amount of [Cp_2Fe][BPh$_4$], which is insoluble under reaction conditions, ensured that it was fully consumed, which facilitated the isolation of **4**. The unreacted **3** was removed by the pentane washes. ^{1}H NMR (C_6D_5F): δ 273.3, 167.5, 17.7, 16.2, 10.9, 3.8, −18.1, −23.9, −35.1, −146.3. HR-ESI-MS (C_6H_5F, positive ion mode) *m/z* 596.2949 ([M − BPh_4^-]$^+$, calcd. for $C_{59}H_{66}BFeN_3O_2$: 596.2934). ESI-MS (C_6H_5F, negative ion mode) *m/z* 319.2 (BPh_4^-). μ_{eff} (SQUID, 27 °C): 5.3 μ_B. Multiple elemental analyses of crystalline samples of **4** gave irreproducible results for C but accurate results for H and N possibly due to incomplete combustion. Anal. Calcd for $C_{59}H_{66}BFeN_3O_2$: C, 77.38; H, 7.26; N, 4.59. Found: C, 74.92; H, 7.54; N, 4.43. IR ν_{CO} (KBr): 1548, 1472 cm^{-1}. IR assignments were made by inspection of the IR spectra of **4**, **4-^{13}C$_1$** (synthesized from **2** and $^{13}CO_2$), and (PDI)FeCl$_2$ (Figure S-11 in the Supporting Information).

Generation of [(PDI)Fe(OAc)THF][BPh$_4$] (4-THF). THF (0.01 mmol) was added by syringe to a solution of **4** (9.1 mg, 0.0099 mmol) in C_6D_5F to generate **4-THF**. The formation of **4-THF** is supported by the ^{1}H NMR spectra of mixtures of **4** and THF, which exhibit resonances at the mole-fraction-weighted average of the chemical shifts of **4** and **4-THF**. These results imply that **4-THF** is formed and exchanges with **4** rapidly on the NMR time scale (see Figure S-3 in the Supporting Information). ^{1}H NMR (C_6D_5F): δ 199.2, 112.9, 12.4, 9.3, 4.3, 2.9, 2.4, 1.2, −1.3, −11.8, −13.7, −16.0, −78.9. ^{1}H NMR (THF-d_8): δ 156.8, 78.7, 13.9, 8.7, 7.8, 7.3, −4.5, −11.1, −13.5, −35.1.

Kinetic Analysis of the Reaction of Fe Alkyl Complexes with CO$_2$. An NMR tube was charged with the Fe alkyl complex, and the solvent was added by vacuum transfer at −196 °C. The mixture was warmed to the desired temperature and exposed to CO_2 at the desired pressure. The tube was then rapidly inserted into an NMR probe that had been equilibrated at the desired temperature. ^{1}H NMR spectra were recorded periodically. Specific details for each complex are included in the Supporting Information.

Attempted Reaction of 2-THF-*d*$_8$ with CO$_2$. An NMR tube was charged with **2** (4.8 mg, 0.0055 mmol). THF-d_8 (0.5 mL) was added by vacuum transfer at −196 °C. The mixture was thawed at room temperature, exposed to CO_2 (1 atm, 19 equiv), and allowed to stand at room temperature for 2 days. ^{1}H NMR spectra were recorded and showed that **2-THF-*d*$_8$** had partially decomposed to the same unidentified products at approximately the same rate as in the absence of CO_2. There was no evidence for the formation of [(PDI)Fe(OAc)-(THF-d_8)][BPh$_4$] (**4-THF-*d*$_8$**).

■ ASSOCIATED CONTENT

Supporting Information

The Supporting Information is available free of charge on the ACS Publications website at DOI: 10.1021/acs.organomet.6b00470.

Additional experimental details, NMR and IR spectra, X-ray diffraction data, SQUID data, EPR spectra, figures, and tables (PDF)

Crystallographic data for **1-PMe$_3$** and **4** (CIF)

■ AUTHOR INFORMATION

Corresponding Author

*E-mail: rfjordan@uchicago.edu.

Notes

The authors declare no competing financial interest.

■ ACKNOWLEDGMENTS

This work was supported by the National Science Foundation (CHE-0911180 and CHE-1048528) and the University of Chicago Women's Board. We thank Drs. Antoni Jurkiewicz and C. Jin Qin for assistance with NMR spectroscopy and mass spectrometry, respectively, Drs. Ian Steele and Alexander Filatov for assistance with X-ray diffraction, and Prof. John Anderson and Airi Kawamura for SQUID measurements and EPR spectroscopy.

■ REFERENCES

(1) Reviews: (a) Darensbourg, D. J.; Kudaroski, R. *Adv. Organomet. Chem.* **1983**, *22*, 129. (b) Aresta, M.; Dibenedetto, A. *Dalton Trans.* **2007**, 2975. (c) Correa, A.; Martin, R. *Angew. Chem., Int. Ed.* **2009**, *48*, 6201. (d) Zhang, Y.; Riduan, S. N. *Angew. Chem., Int. Ed.* **2011**, *50*, 6210. (e) Tsuji, Y.; Fujihara, T. *Chem. Commun.* **2012**, *48*, 9956. (f) Maeda, C.; Miyazaki, Y.; Ema, T. *Catal. Sci. Technol.* **2014**, *4*, 1482. (g) Liu, Q.; Wu, L.; Jackstell, R.; Beller, M. *Nat. Commun.* **2015**, *6*, 5933.

(2) Catalytic reactions involving CO_2 insertion into M−alkyl bonds: (a) Williams, C. M.; Johnson, J. B.; Rovis, T. *J. Am. Chem. Soc.* **2008**,

130, 14936. (b) Ohmiya, H.; Tanabe, M.; Sawamura, M. *Org. Lett.* **2011**, *13*, 1086. (c) Ohishi, T.; Zhang, L.; Nishiura, M.; Hou, Z. *Angew. Chem., Int. Ed.* **2011**, *50*, 8114. (d) León, T.; Correa, A.; Martin, R. *J. Am. Chem. Soc.* **2013**, *135*, 1221. (e) Liu, Y.; Cornella, J.; Martin, R. *J. Am. Chem. Soc.* **2014**, *136*, 11212. (f) Moragas, T.; Gaydou, M.; Martin, R. *Angew. Chem., Int. Ed.* **2016**, *55*, 5053. (g) Börjesson, M.; Moragas, T.; Martin, R. *J. Am. Chem. Soc.* **2016**, *138*, 7504.

(3) Catalytic reactions involving CO_2 insertion into other M−C bonds: (a) Zhang, L.; Cheng, J.; Ohishi, T.; Hou, Z. *Angew. Chem., Int. Ed.* **2010**, *49*, 8670. (b) Mizuno, H.; Takaya, J.; Iwasawa, N. *J. Am. Chem. Soc.* **2011**, *133*, 1251. (c) Ohishi, T.; Zhang, L.; Nishiura, M.; Hou, Z. *Angew. Chem., Int. Ed.* **2011**, *50*, 8114. (d) Fujihara, T.; Nogi, K.; Xu, T.; Terao, J.; Tsuji, Y. *J. Am. Chem. Soc.* **2012**, *134*, 9106. (e) Moragas, T.; Cornella, J.; Martin, R. *J. Am. Chem. Soc.* **2014**, *136*, 17702. (f) Wang, X.; Liu, Y.; Martin, R. *J. Am. Chem. Soc.* **2015**, *137*, 6476. (g) Rebih, F.; Andreini, M.; Moncomble, A.; Harrison-Marchand, A.; Maddaluno, J.; Durandetti, M. *Chem.—Eur. J.* **2016**, *22*, 3758.

(4) (a) Hill, M.; Wendt, O. *Organometallics* **2005**, *24*, 5772. (b) Lau, K.-C.; Petro, B. J.; Bontemps, S.; Jordan, R. F. *Organometallics* **2013**, *32*, 6895.

(5) (a) LeBlanc, F. A.; Berkefeld, A.; Piers, W. E.; Parvez, M. *Organometallics* **2012**, *31*, 810. (b) Kloppenburg, L.; Petersen, J. L. *Organometallics* **1996**, *15*, 7. (c) Zucchini, U.; Albizzati, E.; Giannini, U. *J. Organomet. Chem.* **1971**, *26*, 357.

(6) Hartwig, J. F.; Bergman, R. G.; Andersen, R. A. *J. Am. Chem. Soc.* **1991**, *113*, 6499.

(7) (a) Johansson, R.; Jarenmark, M.; Wendt, O. F. *Organometallics* **2005**, *24*, 4500. (b) Johnson, M. T.; Johansson, R.; Kondrashov, M. V.; Steyl, G.; Ahlquist, M. H. G.; Roodt, A.; Wendt, O. F. *Organometallics* **2010**, *29*, 3521. (c) Schmeier, T. J.; Hazari, N.; Incarvito, C. D.; Raskatov, J. A. *Chem. Commun.* **2011**, *47*, 1824. (d) Schmeier, T. J.; Nova, A.; Hazari, N.; Maseras, F. *Chem.—Eur. J.* **2012**, *18*, 6915. (e) Jonasson, K. J.; Wendt, O. *Chem.—Eur. J.* **2014**, *20*, 11894.

(8) (a) Darensbourg, D. J.; Rokicki, A. *J. Am. Chem. Soc.* **1982**, *104*, 349. (b) Darensbourg, D. J.; Kudaroski, R. *J. Am. Chem. Soc.* **1984**, *106*, 3672. (c) Darensbourg, D. J.; Hanckel, R. K.; Bauch, C. G.; Pala, M.; Simmons, D.; White, J. N. *J. Am. Chem. Soc.* **1985**, *107*, 7463. (d) Darensbourg, D. J.; Grotsch, G. *J. Am. Chem. Soc.* **1985**, *107*, 7473. Carboxylation of metal hydrides: (e) Darensbourg, D. J.; Rokicki, A.; Darensbourg, M. Y. *J. Am. Chem. Soc.* **1981**, *103*, 3223. (f) Darensbourg, D. J.; Rokicki, A. *Organometallics* **1982**, *1*, 1685. (g) Darensbourg, D. J.; Wiegreffe, P. W.; Riordan, C. G. *J. Am. Chem. Soc.* **1990**, *112*, 5759. (h) Darensbourg, D. J.; Wiegreffe, H. P.; Wiegreffe, P. W. *J. Am. Chem. Soc.* **1990**, *112*, 9252.

(9) (a) Allen, O. R.; Dalgarno, S. J.; Field, L. D.; Jensen, P.; Willis, A. C. *Organometallics* **2009**, *28*, 2385. (b) Darensbourg, D. J.; Kyran, S. J.; Yeung, A. D.; Bengali, A. A. *Eur. J. Inorg. Chem.* **2013**, *2013*, 4024.

(10) (a) Darensbourg, D. J.; Groetsch, G.; Wiegreffe, P.; Rheingold, A. L. *Inorg. Chem.* **1987**, *26*, 3827. (b) Ostapowicz, T. G.; Hölscher, M.; Leitner, W. *Chem.—Eur. J.* **2011**, *17*, 10329.

(11) (a) Ikariya, T.; Yamamoto, A. *J. Organomet. Chem.* **1974**, *72*, 145. (b) Miyasuta, A.; Yamamoto, A. *J. Organomet. Chem.* **1976**, *113*, 187. (c) Marsich, N.; Camus, A.; Nardin, G. *J. Organomet. Chem.* **1982**, *239*, 429. (d) Sakaki, S.; Ohkubo, K. *Organometallics* **1989**, *8*, 2970. (e) Sakaki, S.; Musashi, Y. *Inorg. Chem.* **1995**, *34*, 1914. (f) Mankad, M. P.; Gray, T. G.; Laitar, D. S.; Sadighi, J. P. *Organometallics* **2004**, *23*, 1191. (g) Dang, L.; Lin, Z.; Marder, T. B. *Organometallics* **2010**, *29*, 917.

(12) (a) Bianchini, C.; Giambastiani, G.; Rios, I. G.; Mantovani, G.; Meli, A.; Segarra, A. M. *Coord. Chem. Rev.* **2006**, *250*, 1391. (b) Small, B. L.; Brookhart, M.; Bennett, A. M. A. *J. Am. Chem. Soc.* **1998**, *120*, 4049. (c) Britovsek, G. J. P.; Gibson, V. C.; Kimberley, B. S.; Maddox, P. J.; McTavish, S. J.; Solan, G. A.; White, A. J. P.; Williams, D. J.; Britovsek, G. J. P. *Chem. Commun.* **1998**, 849. (d) Small, B. M.; Brookhart, M. *J. Am. Chem. Soc.* **1998**, *120*, 7143. (e) Britovsek, G. J. P.; Bruce, M.; Gibson, V. C.; Kimberley, B. S.; Maddox, P. J.; Mastroianni, S.; McTavish, S. J.; Redshaw, C.; Solan, G. A.; Strömberg, S.; White, A. J. P.; Williams, D. J. *J. Am. Chem. Soc.* **1999**, *121*, 8728.

(13) (a) Bart, S. C.; Lobkovsky, E.; Chirik, P. J. *J. Am. Chem. Soc.* **2004**, *126*, 13794. (b) Tondreau, A. M.; Atienza, C. C. H.; Weller, K. J.; Nye, S. A.; Lewis, K. M.; Delis, J. G. P.; Chirik, P. J. *Science* **2012**, *335*, 567. (c) Tondreau, A. M.; Atienza, C. C. H.; Darmon, J. M.; Milsmann, C.; Hoyt, H. M.; Weller, K. J.; Nye, S. A.; Lewis, K. M.; Boyer, J.; Delis, J. G. P.; Lobkovsky, E.; Chirik, P. J. *Organometallics* **2012**, *31*, 4886. (d) Obligacion, J. V.; Chirik, P. J. *Org. Lett.* **2013**, *15*, 2680. (e) Bouwkamp, M. W.; Bowman, A. C.; Lobkovsky, E.; Chirik, P. J. *J. Am. Chem. Soc.* **2006**, *128*, 13340. (f) Hoyt, J. M.; Schmidt, V. A.; Tondreau, A. M.; Chirik, P. J. *Science* **2015**, *349*, 960. (g) Sylvester, K. T.; Chirik, P. J. *J. Am. Chem. Soc.* **2009**, *131*, 8772.

(14) (a) Ittel, S. D.; Tolman, C. A.; English, A. D.; Jesson, J. P. *J. Am. Chem. Soc.* **1978**, *100*, 7577. (b) Arafa, I. M.; Shin, K.; Goff, H. M. *J. Am. Chem. Soc.* **1988**, *110*, 5228. (c) Allen, O. R.; Dalgarno, S. J.; Field, L. D.; Jensen, P.; Turnbull, A. J.; Willis, A. C. *Organometallics* **2008**, *27*, 2092. (d) Roth, C. E.; Dibenedetto, A.; Aresta, M. *Eur. J. Inorg. Chem.* **2015**, *2015*, 5066.

(15) Bouwkamp, M. W.; Bart, S. C.; Hawrelak, E. J.; Trovitch, R. J.; Lobkovsky, E.; Chirik, P. J. *Chem. Commun.* **2005**, 3406.

(16) Tondreau, A. M.; Milsmann, C.; Patrick, A. D.; Hoyt, H. M.; Lobkovsky, E.; Wieghardt, K.; Chirik, P. J. *J. Am. Chem. Soc.* **2010**, *132*, 15046.

(17) (a) Bart, S. C.; Chlopek, K.; Bill, E.; Bouwkamp, M. W.; Lobkovsky, E.; Neese, F.; Wieghardt, K.; Chirik, P. J. *J. Am. Chem. Soc.* **2006**, *128*, 13901. See also: (b) de Bruin, B.; Bill, E.; Bothe, E.; Weyhermüller, T.; Wieghardt, K. *Inorg. Chem.* **2000**, *39*, 2936. (c) Budzelaar, P. H. M.; de Bruin, B.; Gal, A. W.; Wieghardt, K.; van Lenthe, J. H. *Inorg. Chem.* **2001**, *40*, 4649.

(18) Trovitch, R. J.; Lobkovsky, E.; Chirik, P. J. *J. Am. Chem. Soc.* **2008**, *130*, 11631.

(19) (a) Slejko, F. L.; Drago, R. S.; Brown, D. G. *J. Am. Chem. Soc.* **1972**, *94*, 9210. (b) Rose, N. J.; Drago, R. S. *J. Am. Chem. Soc.* **1959**, *81*, 6138.

(20) Trovitch, R. J.; Lobkovsky, E.; Bouwkamp, M. W.; Chirik, P. J. *Organometallics* **2008**, *27*, 6264.

(21) Deacon, G. B.; Phillips, R. J. *Coord. Chem. Rev.* **1980**, *33*, 227.

(22) Bouwkamp, M. W.; Lobkovsky, E.; Chirik, P. J. *J. Am. Chem. Soc.* **2005**, *127*, 9660.

(23) (a) Jolly, W. L. *The Synthesis and Characterization of Inorganic Compounds*; Prentice-Hall: Englewood Cliffs, NJ, 1970; p 487. (b) Jordan, R. F.; LaPointe, R. E.; Bajgur, C. S.; Echols, S. F.; Willett, R. *J. Am. Chem. Soc.* **1987**, *109*, 4111.

(24) Stoll, S.; Schweiger, A. *J. Magn. Reson.* **2006**, *178*, 42.